Biomaterials 35 (2014) 4185–4194

Contents lists available at ScienceDirect

Biomaterials

journal homepage: www.elsevier.com/locate/biomaterials

Controlled release of doxorubicin from graphene oxide based charge-reversal nanocarrier

Ting Zhou, Xiaoming Zhou*, Da Xing*

MOE Key Laboratory of Laser Life Science & Institute of Laser Life Science, College of Biophotonics, South China Normal University, Guangzhou 510631, China

ARTICLE INFO

Article history:
Received 25 December 2013
Accepted 20 January 2014
Available online 7 February 2014

Keywords:
Graphene oxide
Charge-reversal polyelectrolyte
Drug delivery
Cancer cell targeted
pH-responsive release

ABSTRACT

A number of anticancer drugs, such as doxorubicin (DOX), operate only after being transported into the nucleus of cancer cells. Thus it is essential for the drug carriers to effectively release the anticancer drugs into the cytoplasm of cancer cells and make them move to nucleus freely. Herein, a pH-responsive charge-reversal polyelectrolyte and integrin $\alpha_V\beta_3$ mono-antibody functionalized graphene oxide (GO) complex is constituted as a nanocarrier for targeted delivery and controlled release of DOX into cancer cells. The DOX loading and releasing *in vitro* demonstrates that this nanocarrier cannot only load DOX with high efficiency, but also effectively release it under mild acidic pH stimulation. Cellular toxicity assay, confocal laser scanning microscopy and flow cytometer analysis results together confirm that with the targeting nanocarrier, DOX can be selectively transported into the targeted cancer cells. Then they will be effectively released from the nanocarriers in cytoplasm and moved into the nucleus subsequently, stimulating by charge-reverse of the polyelectrolyte in acidic intracellular compartments. The effective delivery and release of the anticancer drugs into nucleus of the targeted cancer cells will lead to a high therapeutic efficiency. Hence, such a targeting nanocarrier prepared from GO and charge-reversal polyelectrolytes is likely to be an available candidate for targeted drug delivery in tumor therapy.

1. Introduction

The ideal effect for controlled drug delivery is for the drug to get to a desired therapeutic concentration at targeting sites while at other tissues is kept at safe levels [1–3]. And one of the major challenges to achieve this effect is to find a suitable delivery carrier. An ideal controlled carrier for anti-cancer drugs should have long circulation duration, the ability to target cancer cells, and eventually the ability to efficiently deliver and release drugs into cytoplasm. Currently, various polymeric particles [4–6], liposomes [7–9], microspheres [10,11] and nanoparticles [12–14] have been used as potential antitumor drug carriers. Among these carriers, nanomaterials demonstrate advantages in anti-cancer drug delivery including a tunable circulation life time, enhanced permeability and retention (EPR) effect that up-regulates intratumoral delivery due to the high permeability of tumor vasculatures, and multivalent effect that increases receptor targeting specificity by labeling multiple ligands on a single nanoparticle [15,16].

Recently, graphene oxide (GO) as a promising nanomaterial for drug delivery has attracted significant attentions for its good biocompatibility, endocytosis, and large specific surface area for loading drugs and other functional biomolecules [17–20]. Compared with other drug carriers, GO has much higher loading capacity, which makes it can effectively enhance the drug delivery into cells [17,19,21]. Furthermore, with a lot of active groups such as hydroxyl and carboxyl on the surface of GO, targeting molecules such as folic acid, antibodies can be conveniently immobilized on, and then enable GO to be specifically internalized into the targeted cells [22–24]. Accordingly, with the targeting molecule functional GO as the drug carrier, drugs can be efficiently and selectively transported into the targeted cells.

Doxorubicin (DOX), as a commonly used anticancer drug in chemotherapy, kills cells by intercalating with DNA, thereby preventing the DNA replication and then the cell division process [25,26]. Consequently, it operates only when being sufficiently transported into the nucleus of cancer cells. However, most of the drug carriers so far such as liposomes and nanoparticles, including GO, can neither migrate into the cellar nucleus due to their large size nor effectively release their cargoes in the cytoplasm [27,28]. Then only a small percentage of drugs delivered into the cytoplasm can reach the nucleus eventually. Thus, it is urgent to construct a drug carrier capable of effectively releasing anticancer drugs in the cytoplasm of cancer cells to make the drugs move into the nucleus, leading to a high therapeutic efficiency.

* Corresponding authors.
E-mail addresses: zhouxm@scnu.edu.cn (X. Zhou), xingda@scnu.edu.cn (D. Xing).

0142-9612/$ – see front matter © 2014 Elsevier Ltd. All rights reserved.
http://dx.doi.org/10.1016/j.biomaterials.2014.01.044

Smart structures that are responsive to external stimuli, such as heat, light, pH or magnetic fields are ideal candidates for controlled release of anticancer drug [29–36]. By formulating these stimuli-responsive materials with drug carriers, DOX can be released from the delivery systems in cytoplasm under some specific stimuli, then move into the nucleus to kill cells. Different to the physiological pH (7.4) of normal cells, the extracellular environment of solid tumors is acidic (pH ~ 6.8), and the pH values in endosomes are even a lot lower (5.0–6.5) [32,37,38]. According to this, pH-responsive nanocarriers can be developed to deliver and efficiently release anticancer drugs in cancer cells, because it is reasonable to insert acid-cleavable linkers in a nanocarrier to induce destabilization of the carrier in endosome, resulting in the release of drugs from the nanocarrier into cytoplasm. The charge-reversal polyelectrolyte is a kind of polymer that could pH-dependently shift its charge nature between positive and negative. This property make charge-reversal polyelectrolyte an ideal material to constitute the pH-responsive nanocarriers for releasing the anticancer drugs, siRNA, genes and proteins in cytoplasm [39–45]. As an anionic carboxylate-functional polyelectrolyte, citraconic anhydride-functionalized poly(allylamine) (PAH-Cit) is a common charge-reversal polyelectrolyte, which can be readily converted back to cationic poly(allylamine) by amide hydrolysis upon exposure to mild acidic environments (Scheme 1A), such as those found within late endosomes and lysosomes [39,40,46].

Herein, we developed a GO based charge-reversal nanocarrier (GO-Abs/PEI/PAH-Cit/DOX) for enhanced delivery and controlled release of DOX into specific cancer cells. PAH-Cit was conjugated with a cationic polyelectrolyte (polyethyleneimine, PEI) coated GO by electrostatics. And DOX was loaded on GO by covalently linkage with PAH-Cit. As shown in Scheme 1A and C, after the drug delivery system is endocytosed into cells, the PAH-Cit/DOX will convert to cationic poly(allylamine) upon exposure to acidic environments of endosome or lysosome. Hence it is released from the positive charge surface of GO/PEI. It will be expected that this nanocarrier can specifically transport anti-cancer drugs into the targeted cancer cells with high efficiency, and then release them to move into nucleus to achieve the medical effect.

2. Experimental section

2.1. Materials and characterization

Citraconic anhydride and polyethyleneimine (PEI, M_w ~ 60 KDa) were purchased from TCI Tokyo Chemical Industry Co.,Ltd; Doxorubicin hydrochloride (DOX), poly (allyamine hydrochloride) (PAH, M_w ~ 15 kDa), N-hydroxy succinimide (NHS) and 1-ethyl-3-(3-dimethylaminopropyl) carbodiimide hydrochloride (EDC) were purchased from Sigma–Aldrich Co. Integrin $\alpha_V\beta_3$ (23C6) mono-clonal antibody (integrin $\alpha_V\beta_3$ mAb) was purchased from Santa Cruz Biotechnology Inc. (Santa Cruz, CA, USA); CCK-8 was purchased from Dojindo Laboratories (Kumamoto, Japan). The graphene oxide (GO) was the product of XF NANO, INC (Nanjing, China). Since all the chemicals were analytical grade and were used without further purification. The high-purity deionized water (resistance >18 MΩ cm) is used throughout.

The optical absorbance characteristics of various samples were investigated by visible absorption spectra (Lambda-35 UV–Vis spectrophotometer, Perkin–Elmer, USA) and fluorescence spectra (LS-55 fluorescence spectrophotometer, Perkin–Elmer, USA) with an excitation of 490 nm. Tapping mode atomic force microscopy (Agilent 5500AFM) purchased from Agilent Technologies, Inc. (Englewood, USA) was used for detecting the size of GO and GO/PEI/PAH-Cit/DOX. The zeta potential of various samples were measured by affordable molecular/particle size and zeta potential analyzer (Malvern instruments, Zetasizer Nano-ZS) at 25 °C, and all the samples were dispersed in phosphate buffer solution (PBS) of pH 7.4.

2.2. Synthesis of charge-reversal polyelectrolyte and the conjugation of DOX

We synthesized the charge-reversal polyelectrolyte according to the Lynn [46]. PAH (40 mg) was dissolved in NaOH (1 M) and stirred for several hours. Citraconic anhydride was then added dropwise into the PAH solution, with NaOH (6 M) added during the reaction to keep the pH above 8.0. After overnight reaction, the resultant mixture was filtrated through 3 kDa filters (Millipore) to remove excess reagents. Then 100 μL of 5 M DOX was put into the 1 mL as-prepared polyelectrolyte, followed by 100 μL of EDC and 100 μL of NHS added to the resultant solution in succession to catalyze the attachment of DOX to the polyelectrolyte. The mixture was incubated for 24 h, protected from light illumination. Unbound excess DOX was also removed by filtration through 3 kDa filters (Millipore) and repeated rinsing.

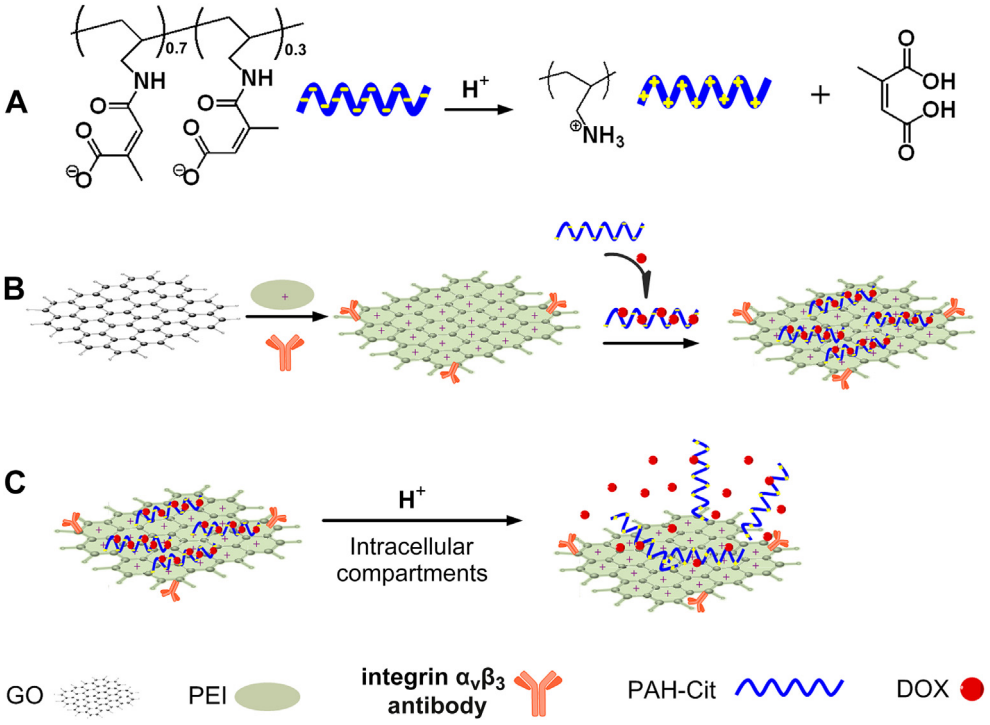

Scheme 1. (A) Hydrolysis of the citraconic amide side chains of anionic charge-reversal polyelectrolyte (PAH-Cit) under mild acidic conditions yields cationic PAH (poly(allylamine)). (B) Construction of the targeted charge-reversal nanocarrier (GO-Abs/PEI/PAH-Cit/DOX). (C) Controlled release of DOX at endosome or lysosome, stimulating by the pH-dependent charge-reverse of the charge-reversal polyelectrolytes on GO.

2.3. Preparation of the nanocarriers

2.3.1. GO/PEI/PAH-Cit/DOX

GO was carboxylated using a modified protocol [18,47]. After NaOH (0.1 g) and chloroacetic acid ($ClCH_2COOH$) (0.1 g) were added, 1 mL GO suspension was bath sonicated at 80 °C for 3 h to convert −OH groups to −COOH groups. The resulting mixture was centrifuged twice at 13,000 rpm. The supernatant was disregarded and the resulting particles were redispersed in pure water. Then 100 μL of PEI solution, EDC (20 mM) and NHS (20 mM) were dropwise added in succession. After 24 h reaction, the mixture was centrifuged at 13,000 rpm for 10 min. Then the nanocarriers were constructed by adding the DOX conjugated charge-reversal polyelectrolyte (PAH-Cit/DOX). Finally, after being mixed and stirred for 3 h at room temperature, the solution was centrifugated twice at 13,000 rpm for 10 min. The resulting particles were redispersed in PBS of pH 7.4.

2.3.2. GO-Abs/PEI/PAH-Cit/DOX

Integrin $\alpha_V\beta_3$ mono-clonal antibody was bounded on carboxylated GO by the covalently linkage of carboxyl group with amino group, with EDC and NHS to accelerate the reaction. Then the GO-Abs was assembled as above.

2.3.3. GO-DOX

DOX was covalently attached on carboxylated GO also by the covalently linkage of carboxyl group with amino group, with EDC and NHS to accelerate the reaction.

2.3.4. GO/DOX

DOX was physically attached on GO by adding DOX into GO suspension, and stirring for several hours.

2.4. DOX loading and pH dependently releasing

Different concentrations of PAH-Cit/DOX (0.2–3.2 mg/mL of DOX) were stirred with 1 mL GO/PEI (0.2 mg/mL of GO) for 30 min at room temperature. The resultant product was collected by centrifugation at 13,000 rpm. The amount of unbound DOX in the solution was determined by measuring the absorbance at 490 nm using a calibration curve prepared under the same condition (Fig. S1). The drug loading capacity is defined as (weight of DOX loaded on GO carriers/weight of GO carriers). The drug loading efficiency (%) is defined as (weight of DOX loaded on GO carriers/weight of initially added DOX) × 100.

Different samples used for the release experiments were placed into a 500 kDa dialysis chambers, which were dialyzed in 50 mL of pH 5 acetic buffer (the endosomal pH of cancer cells), pH 6.8 phosphate buffer (the pH of cancer tissues), and pH 7.4 phosphate buffer (the physiological pH), stirring inside an incubator shaker at 37 °C respectively. The drug release was assumed to start as soon as the dialysis chambers were placed into the reservoirs. The release reservoirs were kept under constant stirring, and at various time points, 100 μL of the solution in the release reservoirs was taken out for characterization. The concentration of DOX released from GO was measured by fluorescence at 600 nm using a calibration curve prepared under the same condition (Fig. S2).

2.5. Cell culture and animal model

U87 MG human glioblastoma cancer cells and MCF-7 human breast cancer cells were cultured in Eagle's minimal essential medium (EMEM) and Dulbecco's modified Eagle's medium (DMEM), respectively. The media were supplemented with 10% fetal bovine serum (FBS) and 1% penicillin–streptomycin, in 5% CO_2, 95% air at 37 °C in a humidified incubator. Female Balb/c mice, aged 6–8 weeks were used for *in vivo* pharmacokinetic studies. The U87 MG tumors were generated by subcutaneous injection of 1×10^7 cells in 100 μL PBS to female athymic nude mice. After 14 days of xenograft, tumor-bearing nude mice were sacrificed for biodistribution experiments.

2.6. Cellular toxicity by CCK8 assay

U87 MG cells were seeded in 96-well plates at 1×10^4 cells per well and subsequently transfected with GO/PEI/PAH-Cit, free DOX, GO-DOX, GO/PEI/PAH-Cit/DOX and GO-Abs/PEI/PAH-Cit/DOX at the DOX concentration of 1 μM and GO concentration of 1 μg/mL, respectively. After 24, 36 and 48 h incubation, respectively, CCK-8 was added to each well and incubated at 37 °C in 5% CO_2 for 2 h. Then the absorbance of each well at 450 nm was measured by Infinite M200 (TECAN, Mannedorf, Switzerland). The results were expressed as the mean percentage of cell viability relative to untreated cells.

2.7. Cellular uptake and the controlled release of DOX

To verify the targeted cellular uptake and controlled drug release of the charge-reversal nanocarrier, 500 μL of U87 MG cells were incubated with free DOX, GO-DOX, GO-Abs/DOX, GO/PEI/PAH-Cit/DOX and GO-Abs/PEI/PAH-Cit/DOX at 37 °C (5% CO_2), respectively. All the samples are used at the DOX concentration of 0.4 μM. Based on the fluorescence of doxorubicin, these cells were imaged at various time points by a commercial laser scanning microscope (LSM510/ConfoCor2) combination system (Zeiss, Germany) equipped with a Plan-Neo fluar 40×/1.3 NA oil DIC objective. The DOX was excited at 488 nm with an Ar-ion laser (reflected by a beam splitter HFT 488 nm) and the fluorescence emission was recorded through a 560 nm IR long-pass filter.

2.8. Quantification of the fluorescence intensity

To quantify the fluorescence intensity and further confirm the targeting nanocarrier can be selectively internalized into the targeted cancer cells, U87 MG cells and MCF-7 cells were seeded in 12-well plates and subsequently transfected with free DOX, GO-Abs/DOX, GO/PEI/PAH-Cit/DOX and GO-Abs/PEI/PAH-Cit/DOX at the DOX concentration of 0.4 μM. After 2 h incubation, they were rinsed with PBS, and harvested with trypsin. Cells under different treatments were washed and resuspended in ice-cold PBS. The DOX fluorescence histogram of cells was obtained from 10,000 cells by flow cytometry (Becton Dickinson FACScan).

2.9. In vivo pharmacokinetic and biodistribution studies

2.9.1. In vivo pharmacokinetic studies

Free DOX and GO-Abs/PEI/PAH-Cit/DOX in PBS equivalent to 5 mg/kg DOX was administered to Balb/c mice by tail vein injection, respectively. DOX measurement was according to the previously reported protocols with minor modifications [48,49]. After predetermined time intervals, approximately 20 μL of blood was drawn from the tail vein of U87 MG tumor bearing nude mice to measure the blood circulation of DOX. Briefly, the blood samples were dissolved in lysis buffer 1 (defined by 1% sodium dodecylsulfate (SDS), 1% Triton X-100, 40 mM tris(hydroxymethyl)aminomethane (tris) acetate, 10 mM ethylene diamine tetra-acetic acid (EDTA), and 10 mM dithiothreitol (DTT)). Then DOX was extracted by incubating blood samples in 1 mL HCl (0.75 N) in isopropanol at −20 °C overnight. After centrifugation at 15,000 rpm for 20 min, the fluorescence of the supernatant was measured using a fluorescence spectra (LS-55 fluorescence spectrophotometer, Perkin–Elmer, USA).

2.9.2. Biodistribution studies

U87 MG tumor bearing nude mice were sacrificed at 30 min and 6 h after tail vein injection with GO-Abs/PEI/PAH-Cit/DOX and free DOX in PBS at a concentration of 5 mg/kg DOX. The organs/tissues (0.1–0.3 g wet-weight of each) were homogenized in 0.5 mL of lysis buffer 2 (defined by 0.25 M sucrose, 40 mM tris-acetate, 10 mM EDTA). For DOX concentrations detection, 200 μL of each tissue lysates was mixed with 100 μL of 10% Titron X-100. After strong vortexing, DOX was extracted by adding the samples into 1 mL of the extraction solution (0.75 N HCl in isopropanol) and then incubating at −20 °C overnight. Then after centrifugation at 15,000 rpm for 20 min, the fluorescence of the supernatant was measured.

3. Result and discussion

3.1. Synthesis and characterization of the charge-reversal polyelectrolyte functional nanocarrier

The targeting nanocarrier GO-Abs/PEI/PAH-Cit/DOX was prepared as outlined in Scheme 1B. After carboxylation of GO, integrin $\alpha_V\beta_3$ mono-clonal antibodies and PEI were bound on it through the covalent linkage of carboxyl group with amino group. And DOX was conjugated with anionic PAH-Cit by the same chemical linkage. Then, the drug delivery nanosystem was constructed with PAH-Cit/DOX being loaded on the positive charge surface of GO/PEI by electrostatic attraction. We also prepared GO/PEI/PAH-Cit/DOX, GO-DOX and GO/DOX as controls. It was found that GO without any modification was ~100 to 1000 nm in size (Fig. 1A), whereas GO/PEI/PAH-Cit/DOX was decreased to ~20 to 200 nm (Fig. 1C) due to the sonication steps [18,19,50]. And more importantly, the height of GO/PEI/PAH-Cit/DOX increased evidently compared with unmodified GO (Fig. 1B and D), resulting from the layer-by-layer coating of the polymers.

The functionalization process of DOX loaded nanocarriers were determined by UV–Vis spectrophotometer, fluorescent spectrophotometer and atomic force microscopy (AFM). As shown in Fig. 1C and D, containing the same concentration of DOX, the DOX conjugated charge-reversal polyelectrolyte (PAH-Cit/DOX) has nearly the same absorbance and fluorescent characteristics as free DOX, apart from that the peak of plasmon absorbance (λ_{max}) in UV–vis spectra shifted from 488 nm to 501 nm (Fig. 1E). While when the PAH-Cit/DOX was loaded on GO through PEI to form the nanocarrier GO/PEI/PAH-Cit/DOX, the peak shifted further to 556 nm

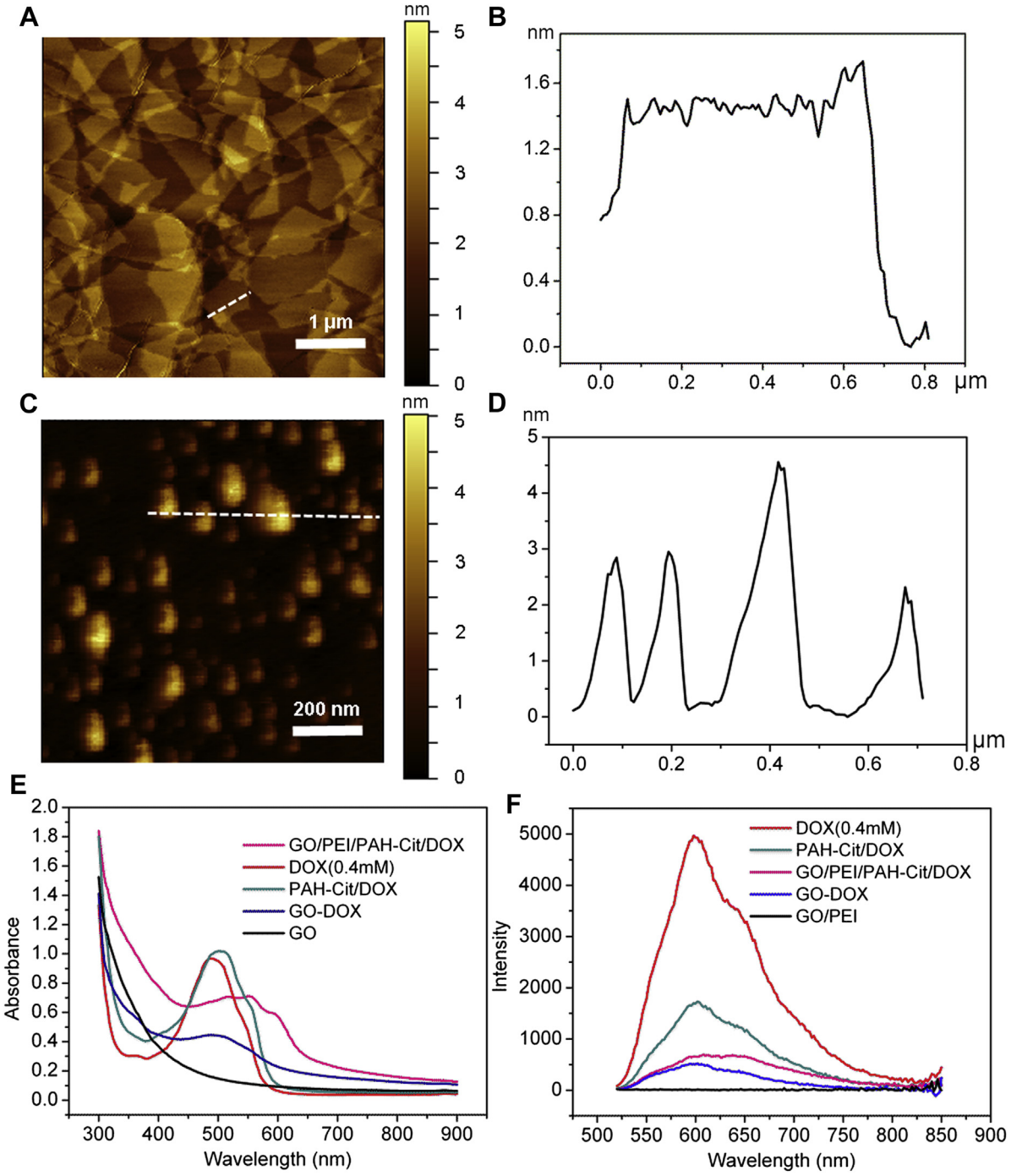

Fig. 1. AFM images and height profiles of GO (A, B) and GO/PEI/PAH-Cit/DOX (C, D). (E) UV–Vis absorbance spectra of DOX, GO, PAH-cit/DOX and GO/PEI/PAH-cit/DOX. (F) Fluorescence spectra of DOX, GO/PEI, PAH-Cit/DOX and GO/PEI/PAH-cit/DOX at the 490 nm excitation wavelength.

and the absorption spectrum broadened. And when DOX was covalently conjugated on GO, the absorbance peak of GO-DOX shifted to 508 nm. As to the fluorescence spectra (Fig. 1F), both GO/PEI/PAH-Cit/DOX and GO-DOX have the similar fluorescent characteristic with DOX, though the fluorescent intensity diminished due to the quenching effect of GO. These optical results indicated that DOX had been loaded on the GO based nanocarrier as expected.

Zeta potential measurements after each of the coating steps are also used to monitor and verify the successful deposition of polyelectrolytes (Fig. 2). From Fig. 2A, we can see that the charge-reversal ployelectrolyte (PAH-Cit) is positively charged at pH 7.4. While with the pH decrease of the solution, the positive charge amount of PAH-Cit gradually decreases. At pH 5.0, it has reversed to be negatively charged. As shown in Fig. 2B, at pH 7.4, GO as the core of the delivery system, had a negatively charged surface due to its oxygen groups such as hydroxyl and carboxyl. The carboxylation further increased the negative charges because of the increase of carboxylic groups. And after the deposition of the positively charged polyelectrolyte PEI, surface charge of the whole nanosystem (GO/PEI) became positive. Finally the anionic, pH-responsive charge-reversal polyelectrolyte, PAH-Cit, was

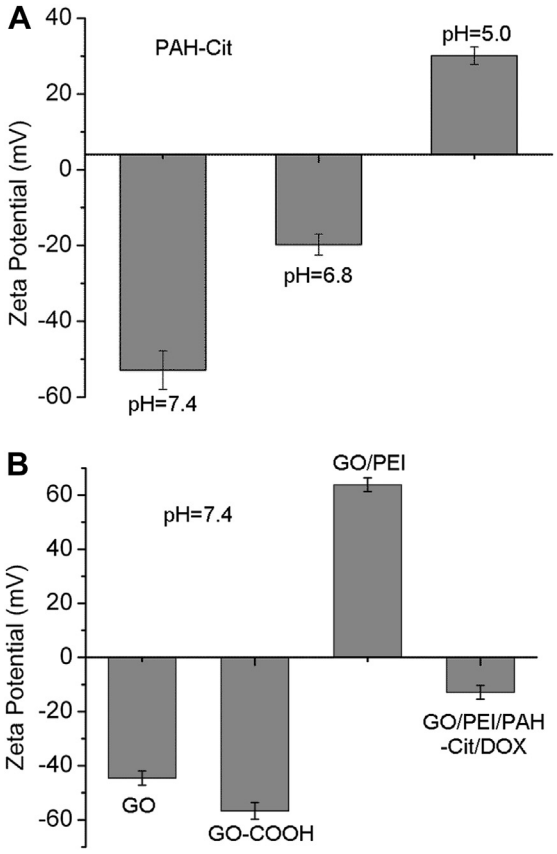

Fig. 2. (A) Zeta-potential change of PAH-Cit under different pH. From pH 7.4 to 5.0, the negative charge nature of PAH-Cit reverses to positive. (B) Zeta-potential of colloidal GO, GO-COOH, GO/PEI and GO/PEI/PAH-Cit/DOX in 0.01 M in PBS buffer at pH 7.4.

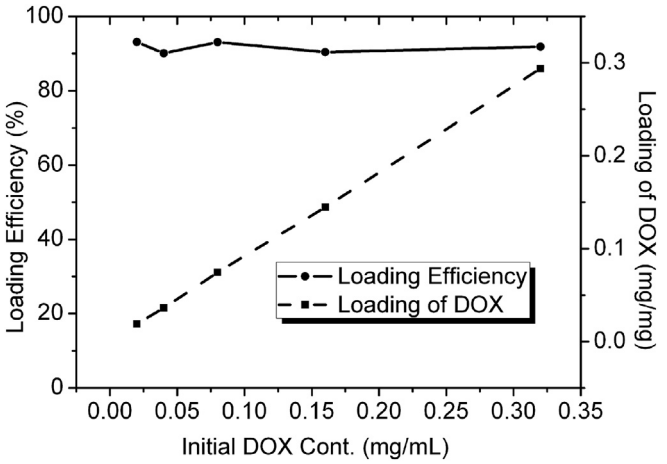

Fig. 3. Drug loading efficiency and drug loading content when 0.2 mg/mL GO is loaded with different initial amount of DOX.

subsequently deposited on the nanosystem through electrostatic attraction, which resulted in the negative charges on the whole nanocarrier (GO/PEI/PAH-Cit/DOX). In addition, PEI on this nanocarrier can help DOX escape from endosomes due to its proton sponge effect [39,51,52].

3.2. Loading and pH responsive releasing of DOX

With the large specific surface area, GO is supposed to has excellent loading behavior. The loading capacity and loading efficiency of the nanocarrier was calculated by measuring the concentration of unbound drug using the absorbance at 490 nm. As shown in Fig. 3, the DOX loading capacity increased linearly with the increasing of the initial DOX concentration, and it reached to 0.294 mg/mg when the initial DOX concentration was 0.32 mg/mL, which was still far away from being saturated. More importantly, the drug loading efficiency was always over 90% among these initial concentrations of DOX. These results indicated that the GO based nanocarrier can load DOX with exceptionally high loading capacity and efficiency, compared with many other common nanocarriers such as carbon nanotubes and polymeric micelles [5,49,53,54]. Thereby, this GO based charge-reversal nanocarrier is a potential nanocarrier for highly efficient load and delivery of DOX.

To validate that the charge-reversal polyelectrolyte can effectively reverse its charge and then release DOX from GO under the pH stimulus, the drug releasing was investigated at pH 5.0, 6.8 and 7.4, respectively. 37 °C, which is close to the physiological temperature, was chosen for the release response. As shown in Fig. 4A, DOX was released very slowly from the nanocarrier at neutral conditions (pH = 7.4). There was only about 28.75% of the total bound released for 24 h. While when pH decreased, the release efficiency of DOX enhanced evidently. After 24 h dialysis, nearly 50.25% of the total DOX was released from the nanocarrier under the pH of tumor tissues (pH = 6.8). And the release efficiency was even up to 81.25% under the endosomal pH of cancer cells (pH = 5.0). Especially in 6 h, DOX released significantly faster under pH = 5.0 than did under other two pH conditions. The results indicated that the release of DOX from the charge-reversal nanocarrier was pH-responsive. And the drug release rate of the nanocarrier at mild acidic pH was significantly higher than at neutral pH. Furthermore, Fig. 4B and C present that the release of DOX form the other ways attached GO, including directly binding on GO with covalent linkages or π−π stacking interactions, is not so pH dependent as from the charge-reversal polyelectrolyte functional GO. Generally, DOX can be loaded on the charge-reversal polyelectrolyte functional GO under physiological conditions and released at reduced pH, typical of micro-environments of cancerous tissues, intracellular lysosomes or endosomes, provides an ideal mechanism for selective drug release.

3.3. In vitro cytotoxicity studies of the DOX loaded nanocarriers

Cytotoxicity to the targeted cancer cells of various DOX loaded drug carriers was investigated using CCK-8 assay. U87 MG cells were used in this experiment because they over-express the used targeted molecule, integrin $\alpha_V\beta_3$. GO/PEI/PAH-Cit, free DOX, GO-DOX, GO/PEI/PAH-Cit/DOX and GO-Abs/PEI/PAH-Cit/DOX with equivalent concentration of GO and DOX were injected into U87 MG cells, respectively. After 24, 36 and 48 h incubation, the cell viability was measured. As we can see from Fig. 5, enhanced cell killing was evidenced in the cells treated with charge-reversal nanocarriers compared to in that with covalently conjugated GO-DOX. That is because DOX can be more effectively released from the charge-reversal nanocarrier than from the GO-DOX. In addition, it was demonstrated that the targeting drug carrier, GO-Abs/PEI/PAH-Cit/DOX, had stronger cytotoxicity than did the non-targeting one, which suggested the potential of selectively internalization and killing of specific cancer cells for the targeting drug carrier. It is also presented in Fig. 5 that free DOX also has a strong cell killing effect for U87 MG cell. However, considering it cannot discriminate normal cells from the cancer cells, it might cause side effects during the cancer therapy. Then targeting drug carriers can be developed to avoid the side effects of free DOX.

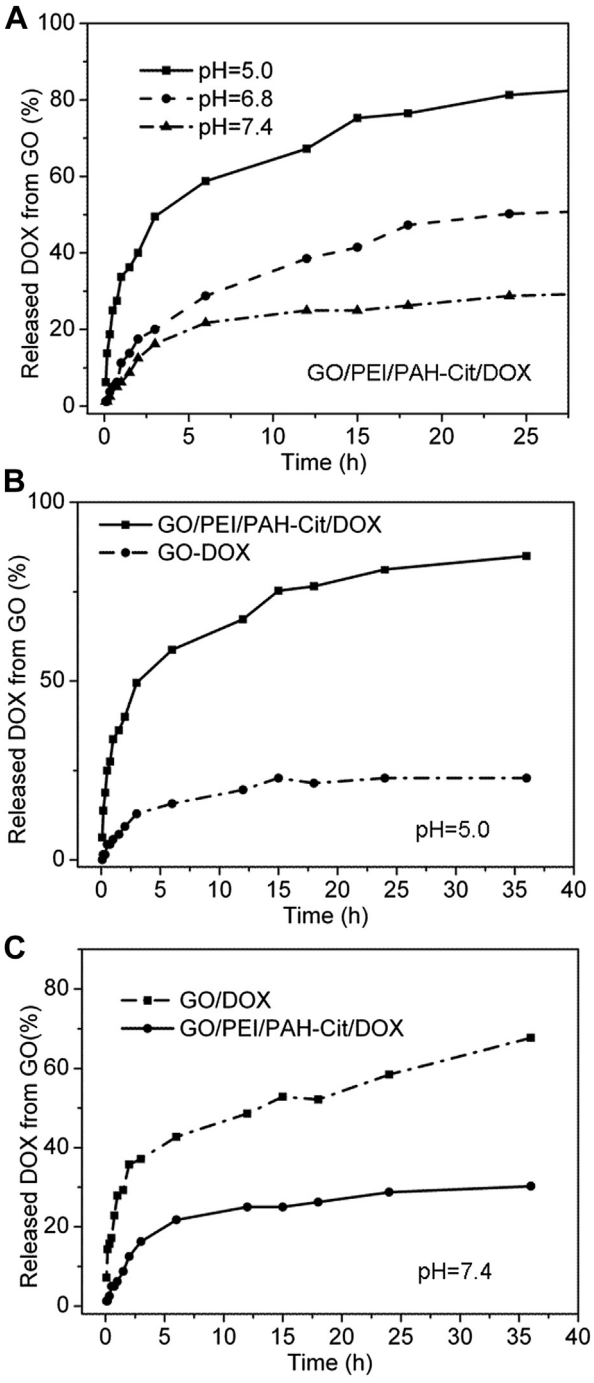

Fig. 4. (A) Cumulative DOX release from the charge-reversal polyelectrolyte coated nanocarriers GO/PEI/PAH-Cit/DOX at pH 5.0, 6.8 and 7.4. (B) Comparison of the cumulative DOX release from GO/PEI/PAH-Cit/DOX and GO-DOX at pH 5.0. (C) Comparison of the cumulative DOX release from GO/PEI/PAH-Cit/DOX and GO/DOX at pH 7.4.

3.4. Pharmacokinetics and biodistribution of the charge-reversal nanocarrier

To investigate the *in vivo* pharmacokinetics and biodistribution of the charge-reversal nanocarrier, GO-Abs/PEI/PAH-Cit/DOX and free DOX were injected into mice through the tail vein, respectively. As shown in Fig. 6, DOX carried with GO-Abs/PEI/PAH-Cit/DOX showed prolonged half-time in blood circulation, compared with free DOX. The DOX circulation half-time increased from 0.52 h for free DOX to 2.1 h for GO-Abs/PEI/PAH-Cit/DOX. As for the biodistribution shown in Fig. 7, most organs showed greater accumulation of GO-Abs/PEI/PAH-Cit/DOX than of free DOX, especially in the liver and lung. More importantly, after 6 h injection, the tumor uptake of DOX enhanced much for GO-Abs/PEI/PAH-Cit/DOX, compared with that for free DOX. It indicated that GO-Abs/PEI/PAH-Cit/DOX might have better specificity than free DOX for tumor therapy. Despite the high RES (reticulo-endothelial system) uptake, GO-Abs/PEI/PAH-Cit/DOX did not show obvious organ toxicity from histology studies (Fig. S4).

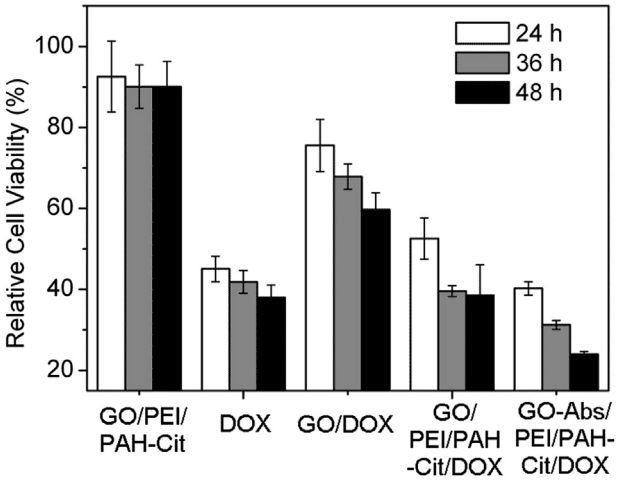

Fig. 5. Relative cellular viability of U87 MG cells after 24 h, 36 h and 48 h treatment with GO/PEI/PAH-Cit, DOX, GO-DOX, GO/PEI/PAH-cit/DOX and GO-Abs/PEI/PAH-cit/DOX, respectively.

3.5. Cell uptake and the controlled release of DOX with the charge-reversal nanocarrier

To further confirm the charge-reversal nanocarrier can selectively transport DOX to the targeted cancer cells, and especially can effectively release the drugs in the cytoplasm, GO-Abs/PEI/PAH-Cit/DOX and other control samples with equivalent DOX concentration

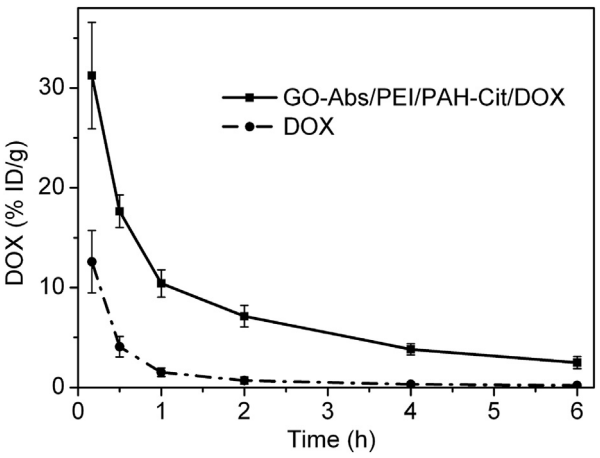

Fig. 6. Pharmacodynamic behavior of GO-Abs/PEI/PAH-Cit/DOX and DOX studied by measuring their blood circulation in mice with fluorescence spectroscopy. GO-Abs/PEI/PAH-Cit/DOX showed prolonged half-time in blood circulation compared with free DOX. Concentrations of DOX in blood were measured at various time points after tail vein injection with GO-Abs/PEI/PAH-Cit/DOX and free DOX (5 mg/kg of DOX concentration). The values plotted are mean ± SD of five experiments.

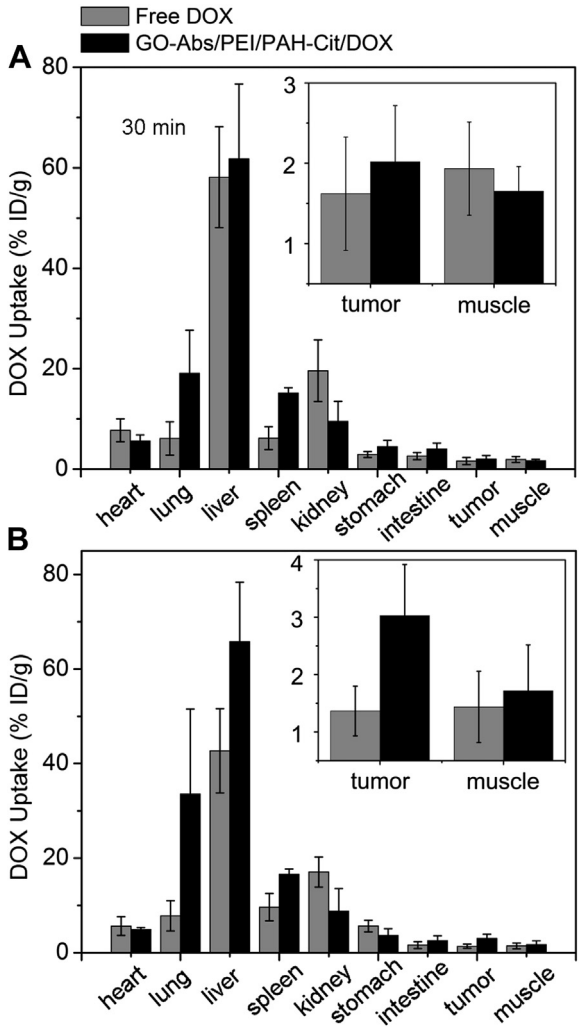

Fig. 7. Biodistribution of DOX and GO-Abs/PEI/PAH-Cit/DOX in major organs at 30 min (A) and 6 h (B) after tail vein injection (5 mg/kg of DOX concentration) into nude mice bearing U87 MG tumor. Most organs showed greater accumulation of GO-Abs/PEI/PAH-Cit/DOX than of free DOX, especially in the liver and lung. After 6 h, the tumor uptake of DOX enhanced much for GO-Abs/PEI/PAH-Cit/DOX, compared with free DOX. The values plotted are mean ± SD of five experiments.

were incubated with U87 MG cells. The intracellular localization of the DOX-loaded nanocarriers was investigated using a confocal fluorescence microscopy on U87 MG cells region soon after entering the cells (Fig. 8A). For the cells treated with free DOX, only after 3 h treatment, the mean fluorescence intensity was much higher in nucleus than in cytoplasm. And almost all the DOX located into the nucleus after 12 h. That is because free DOX can rapidly accumulate inside the cells and ultimately move into the cell nucleus, while the nanocarrier is internalized into cells though the endocytosis pathway and DOX can only migrate into nucleus after the slowly releasing procedure. However, the amount of DOX uptake showed strong pH dependence for the charge-reversal nanocarriers. After 30 min treatment with the charge-reversal nanocarrier, the DOX fluorescence was almost concentrated in the cytoplasm. While after 3 h treatment, the DOX was gradually released from the nanocarriers and moved into the nucleus. And after 12 h, the DOX fluorescence was even stronger in the cytoplasm than in the nucleus. That is attributed to that DOX is gradually released from the nanocarriers in the cytoplasm of U87 MG cells, due to the charge-reversal polyelectrolyte. Nevertheless, the covalently conjugated DOX (GO-DOX) could not be released from GO after 24 h incubation with the cells.

It is worth to mention that the integrin $\alpha_V\beta_3$ mAbs linked nanocarrier was internalized into the targeted U87 MG cells due to the antigen–antibody mediated endocytosis pathway. Consequently, as shown in Fig. 8, more nanocarriers modified with integrin $\alpha_V\beta_3$ mAbs (GO-Abs/PEI/PAH-Cit/DOX and GO-Abs/DOX) can be endocytosed into the U87 MG cells than the nanocarriers without targeting molecules (GO/PEI/PAH-Cit/DOX and GO-DOX). And the targeting nanocarrier was internalized into the U87 MG cells more quickly than the untargeting nanocarriers. The florescence intensity was strong enough only after 30 min treatment of the targeting nanocarriers. While it takes more than 3 h for enough untargeting nanocarriers to be internalized into the cells. The quantitative analysis of the mean fluorescence intensity in nucleus (Fig. 8B) shows the similar results with the fluorescence images. Therefore, it can be concluded from the results that GO-Abs/PEI/PAH-Cit/DOX could be efficiently taken up by U87 MG cells with subsequent intracellular release of DOX, followed by transport of DOX into nucleus with the nanocarrier left in cytoplasm. These properties make the charge-reversal nanocarrier a potential candidate for targeted delivery and controlled release of DOX for cancer treatment.

3.6. *Selective delivery of DOX to targeted cancer cells with the charge-reversal nanocarrier*

To further verify that the targeting charge-reversal nanocarriers can selectively deliver anticancer drugs into the targeted cancer cells, U87 MG cells, which over-express integrin $\alpha_V\beta_3$ on their cell surface, and MCF-7 cells with few integrin $\alpha_V\beta_3$ were chosen in our experiments. After the cells were incubated with free DOX, GO-DOX, GO-Abs/DOX, GO/PEI/PAH-Cit/DOX and GO-Abs/PEI/PAH-Cit/DOX with equivalent concentration of DOX, respectively, the DOX fluorescence intensity of these cells was detected by flow cytometry (Fig. 9). After 2 h incubation with GO-Abs/PEI/PAH-Cit/DOX, much higher fluorescence intensity was observed in U87 MG cells than in MCF-7 cells, indicating that much more DOX was delivered into U87 MG cells than into MCF-7 cells. And at the same time, U87 MG cells treated with GO-Abs/PEI/PAH-Cit/DOX had multiples higher of fluorescence intensity than that with GO/PEI/PAH-Cit/DOX. These results manifested, with integrin $\alpha_V\beta_3$ mono-clonal antibodies, the charge-reversal nanocarrier can be selectively internalized into the targeted cells with higher efficiency. Accordingly, the antibody conjugated nanocarriers can selectively and effectively deliver DOX into the cancer cells highly expressing the corresponding antigen though the antigen–antibody mediated endocytosis pathway.

In addition, as we can see from Fig. 8, GO-Abs/DOX can also be internalized into U87 MG cells with high efficiency. However, from Fig. 9, it is shown that after being incubated with GO-Abs/DOX, both U87 MG cells and MCF-7 cells showed an obvious enhancement in the DOX fluorescence intensity. Therefore the specificity of GO-Abs/DOX for delivery of DOX to the targeted cancer cells is not good as GO-Abs/PEI/PAH-Cit/DOX, due to the pH dependence of its DOX release is weaker so that some DOX might have already been released before entering the cells. These results are in consistent with the pH dependent release experiments (Fig. 4).

4. Conclusions

We successfully functionalized GO with charge-reversal polyelectrolyte and integrin $\alpha_V\beta_3$ mAb for enhanced delivery and controlled release of DOX into specific cancer cells. DOX was demonstrated to be highly efficiently loaded on and released from

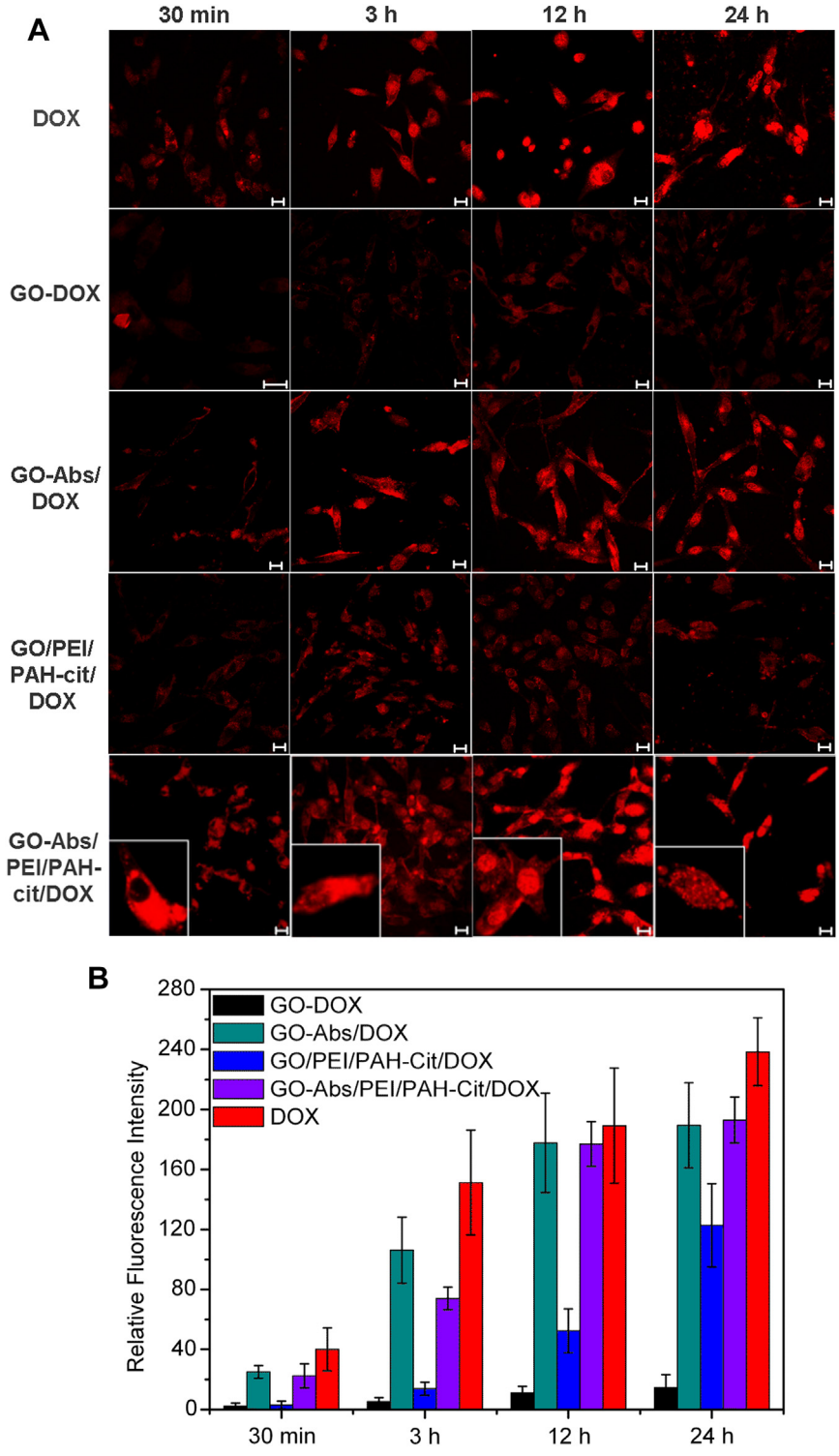

Fig. 8. (A) Confocal fluorescence microscopy images (doxorubicin channel) of U87 MG cells after treated with free DOX, GO-DOX, GO-Abs/DOX, GO/PEI/PAH-Cit/DOX and GO-Abs/PEI/PAH-Cit/DOX with incubation time of 30 min, 3 h, 12 h and 24 h (bar scale = 20 μm), based on the fluorescence of the doxorubicin. Inside the small frames of the GO-Abs/PEI/PAH-Cit/DOX groups are the magnification images of the representative cells of the corresponding regions. (B) Quantitative analysis of the mean fluorescence intensity in the nucleus of U87 MG cells obtained using Laser Scanning Microscope LSM 510 software (Release Version 4.2).

the charge-reversal nanocarrier in the drug loading and releasing experiments. We also confirmed that GO-Abs/PEI/PAH-Cit/DOX could be efficiently taken up by U87 MG cells with subsequent intracellular release of DOX, followed by transporting of DOX into the nucleus with the nanocarrier left in the cytoplasm. On one hand, integrin $\alpha_V\beta_3$ mAbs functional GO as the nanocarrier can load anticancer drugs with high loading capacity and specifically transport them to the targeted cancer cells with high efficiency. On the other hand, the charge-reversal polyelectrolyte on GO make the nanocarrier selectively release the drugs under mild acidic

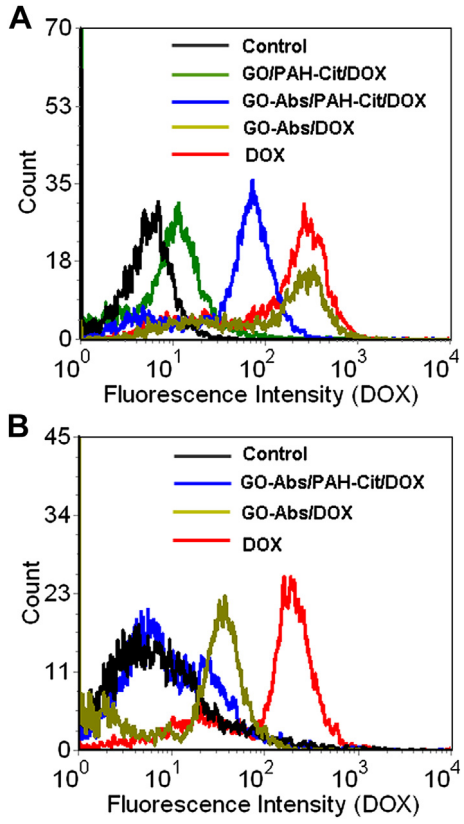

Fig. 9. Fluorescence intensities of integrin $\alpha_v\beta_3$ positive U87 MG cells (A) and integrin $\alpha_v\beta_3$ negative MCF-7 cells (B) obtained with flow cytometry, after these cells were incubated with DOX, GO/PEI/PAHCit/DOX, GO-Abs/PEI/PAH-Cit/DOX and GO-Abs/DOX for 2 h, respectively. The DOX fluorescence histogram of cells was obtained from 10,000 cells by flow cytometry under the 488 nm excitation.

environments of the acidic intracellular organelles such as endosome or lysosome. These properties make the charge-reversal nanocarrier a potential candidate for targeted delivery and controlled release of DOX for cancer treatment.

Acknowledgments

This research is supported by the National Basic Research Program of China (2010CB732602), the Key Program of NSFC-Guangdong Joint Funds of China (U0931005), the National Natural Science Foundation of China (81101121), the Program of the Pear River Young Talents of Science and Technology in Guangzhou, China (2013J2200021) and the Scientific Research Foundation of Graduate School of South China Normal University (2012kyjj122, 2012kyjj117).

Appendix A. Supplementary data

Supplementary data related to this article can be found at http://dx.doi.org/10.1016/j.biomaterials.2014.01.044.

References

[1] Kang B, Li J, Chang S, Dai M, Ren C, Dai Y, et al. Subcellular tracking of drug release from carbon nanotube vehicles in living cells. Small 2012;8:777–82.
[2] Langer R. Drug delivery and targeting. Nature 1998;392:5–10.
[3] Zhang Q, Liu F, Nguyen KT, Ma X, Wang X, Xing B, et al. Multifunctional mesoporous silica nanoparticles for cancer-targeted and controlled drug delivery. Adv Funct Mater 2012;22:5144–56.
[4] Miao Q, Xu D, Wang Z, Xu L, Wang T, Wu Y, et al. Amphiphilic hyper-branched co-polymer nanoparticles for the controlled delivery of anti-tumor agents. Biomaterials 2010;31:7364–75.
[5] Chung JW, Lee KA, Neikirk C, Nelson CM, Priestley RD. Photoresponsive coumarin-stabilized polymeric nanoparticles as a detectable drug carrier. Small 2012;8:1693–700.
[6] Liu P, Yu H, Sun Y, Zhu M, Duan Y. A mPEG-PLGA-b-PLL copolymer carrier for adriamycin and siRNA delivery. Biomaterials 2012;33:4403–12.
[7] Jiang T, Zhang Z, Zhang Y, Lv H, Zhou J, Li C, et al. Dual-functional liposomes based on pH-responsive cell-penetrating peptide and hyaluronic acid for tumor-targeted anticancer drug delivery. Biomaterials 2012;33:9246–58.
[8] Abraham SA, Waterhouse DN, Mayer LD, Cullis PR, Madden TD, Bally MB. The liposomal formulation of doxorubicin. Methods Enzymol 2005;391:71–97.
[9] Wang H, Zhao P, Liang X, Gong X, Song T, Niu R, et al. Folate-PEG coated cationic modified chitosan–cholesterol liposomes for tumor-targeted drug delivery. Biomaterials 2010;31:4129–38.
[10] Son JS, Appleford M, Ong JL, Wenke JC, Kim JM, Choi SH, et al. Porous hydroxyapatite scaffold with three-dimensional localized drug delivery system using biodegradable microspheres. J Control Release 2011;153:133–40.
[11] Gong X, Peng S, Wen W, Sheng P, Li W. Design and fabrication of magnetically functionalized core/shell microspheres for smart drug delivery. Adv Funct Mater 2009;19:292–7.
[12] Wang T, Chai F, Fu Q, Zhang L, Liu H, Li L, et al. Uniform hollow mesoporous silica nanocages for drug delivery *in vitro* and *in vivo* for liver cancer therapy. J Mater Chem 2011;21:5299–306.
[13] Zhang L, Wang T, Lei Y, Liu C, Wang C, Liu H, et al. General route to multifunctional uniform york/mesoporous silica shell nanocapsules: a platform for simultaneous cancer-targeted imaging and magnetically guided drug delivery. Chem Eur J 2012;18:12512–21.
[14] Horcajada P, Chalati T, Serre C, Gillet B, Sebrie C, Baati T, et al. Porous metal-organic-framework nanoscale carriers as a potential platform for drug delivery and imaging. Nat Mater 2010;9:172–8.
[15] Farokhzad OC, Langer R. Impact of nanotechnology on drug delivery. ACS Nano 2009;3:16–20.
[16] Youan BB. Impact of nanoscience and nanotechnology on controlled drug delivery. Nanomedicine 2008;3:401–6.
[17] Geim AK, Novoselov KS. The rise of graphene. Nat Mater 2007;6:183–91.
[18] Sun X, Liu Z, Welsher K, Robinson JT, Goodwin A, Zaric S, et al. Nano-graphene oxide for cellular imaging and drug delivery. Nano Res 2008;1:203–12.
[19] Liu Z, Robinson JT, Sun X, Dai H. PEGylated nanographene oxide for delivery of water-insoluble cancer drugs. J Am Chem Soc 2008;130:10876–7.
[20] Wang C, Li J, Amatore C, Chen Y, Jiang H, Wang XM. Gold nanoclusters and graphene nanocomposites for drug delivery and imaging of cancer cells. Angew Chem Int Ed Engl 2011;50:11644–8.
[21] Chen ML, He YJ, Chen XW, Wang JH. Quantum-dot-conjugated graphene as a probe for simultaneous cancer-targeted fluorescent imaging, tracking, and monitoring drug delivery. Bioconjug Chem 2013;24:387–97.
[22] Huang P, Xu C, Lin J, Wang C, Wang X, Zhang C, et al. Folic acid-conjugated graphene oxide loaded with photosensitizers for targeting photodynamic therapy. Theranostics 2011;1:240–50.
[23] Georgakilas V, Otyepka M, Bourlinos AB, Chandra V, Kim N, Kemp KC, et al. Functionalization of graphene: covalent and non-covalent approaches, derivatives and applications. Chem Rev 2012;112:6156–214.
[24] Wang H, Chen T, Wu S, Chu X, Yu R. A novel biosensing strategy for screening G-quadruplex ligands based on graphene oxide sheets. Biosens Bioelectron 2012;34:88–93.
[25] Momparler RL, Karon M, Siegel SE, Avila F. Effect of adriamycin on DNA, RNA, and protein synthesis in cell-free systems and intact cells. Cancer Res 1976;36:2891–5.
[26] Fornari FA, Randolph JK, Yalowich JC, Ritke MK, Gewirtz DA. Interference by doxorubicin with DNA unwinding in MCF-7 breast tumor cells. Mol Pharmacol 1994;45:649–56.
[27] Timko BP, Dvir T, Kohane DS. Remotely triggerable drug delivery systems. Adv Mater 2010;22:4925–43.
[28] You J, Zhang G, Li C. Exceptionally high payload of doxorubicin in hollow gold nanospheres for near-infrared light-triggered drug release. ACS Nano 2010;4:1033–41.
[29] Wu G, Mikhailovsky A, Khant HA, Fu C, Chiu W, Zasadzinski JA. Remotely triggered liposome release by near-infrared light absorption via hollow gold nanoshells. J Am Chem Soc 2008;130:8175–7.
[30] Lee Y, Fukushima S, Bae Y, Hiki S, Ishii T, Kataoka K. A protein nanocarrier from charge-conversion polymer in response to endosomal pH. J Am Chem Soc 2007;129:5362–3.
[31] Miyata K, Oba M, Nakanishi M, Fukushima S, Yamasaki Y, Koyama H, et al. Polyplexes from poly(aspartamide) bearing 1,2-diaminoethane side chains induce pH-selective, endosomal membrane destabilization with amplified transfection and negligible cytotoxicity. J Am Chem Soc 2008;130:16287–94.
[32] Su J, Chen F, Cryns VL, Messersmith PB. Catechol polymers for pH-responsive, targeted drug delivery to cancer cells. J Am Chem Soc 2011;133:11850–3.
[33] Zhang C, Yang YQ, Huang TX, Zhao B, Guo XD, Wang JF, et al. Self-assembled pH-responsive MPEG-b-(PLA-*co*-PAE) block copolymer micelles for anticancer drug delivery. Biomaterials 2012;33:6273–83.
[34] Dong DW, Xiang B, Gao W, Yang ZZ, Li JQ, Qi XR. pH-responsive complexes using prefunctionalized polymers for synchronous delivery of doxorubicin and siRNA to cancer cells. Biomaterials 2013;34:4849–59.

[35] Yu J, Kuo C, Chen CM, Shin Y, Jyh P. Dual targeted delivery of doxorubicin to cancer cells using folate-conjugated magnetic multi-walled carbon nanotubes. Colloids Surf B Biointerfaces 2012;89:1–9.
[36] Yang X, Zhang X, Ma Y, Huang Y, Wang Y, Chen Y. Super paramagnetic graphene oxide-Fe_3O_4 nanoparticles hybrid for controlled targeted drug carriers. J Mater Chem 2009;19:2710–4.
[37] Yang X, Wang Y, Huang X, Ma Y, Huang Y, Yang R, et al. Multi-functionalized graphene oxide based anticancer drug-carrier with dual-targeting function and pH-sensitivity. J Mater Chem 2011;21:3448–54.
[38] Ding C, Gu J, Qu X, Yang Z. Preparation of multifunctional drug carrier for tumor-specific uptake and enhanced intracellular delivery through the conjugation of weak acid labile linker. Bioconjug Chem 2009;20:1163–70.
[39] Guo S, Huang Y, Jiang Q, Sun Y, Deng L, Liang Z, et al. Enhanced gene delivery and siRNA silencing by gold nanoparticles coated with charge-reversal polyelectrolyte. ACS Nano 2010;4:5505–11.
[40] Han L, Zhao J, Zhang X, Cao W, Hu X, Zou G, et al. Enhanced siRNA delivery and silencing gold-chitosan nanosystem with surface charge-reversal polymer assembly and good biocompatibility. ACS Nano 2012;6:7340–51.
[41] Lee Y, Ishii T, Cabral H, Kim HJ, Seo JH, Nishiyama N, et al. Charge-conversional polyionic complex micelles-efficient nanocarriers for protein delivery into cytoplasm. Angew Chem Int Ed Engl 2009;48:5309–12.
[42] Lee Y, Miyata K, Oba M, Ishii T, Fukushima S, Han M, et al. Charge-conversion ternary polyplex with endosome disruption moiety: a technique for efficient and safe gene delivery. Angew Chem Int Ed Engl 2008;47:5163–6.
[43] Sun B, Lynn DM. Release of DNA from polyelectrolyte multilayers fabricated using 'charge-shifting' cationic polymers: tunable temporal control and sequential, multi-agent release. J Control Release 2010;148:91–100.
[44] Xu P, Van Kirk EA, Zhan Y, Murdoch WJ, Radosz M, Shen Y. Targeted charge-reversal nanoparticles for nuclear drug delivery. Angew Chem Int Ed Engl 2007;46:4999–5002.
[45] Chen T, Shukoor MI, Wang R, Zhao Z, Yuan Q, Bamrungsap S, et al. Smart multifunctional nanostructure for targeted cancer chemotherapy and magnetic resonance imaging. ACS Nano 2011;5:7866–73.
[46] Liu X, Zhang J, Lynn DM. Polyelectrolyte multilayers fabricated from 'charge-shifting' anionic polymers: a new approach to controlled film disruption and the release of cationic agents from surfaces. Soft Matter 2008;4:1688–95.
[47] Wang H, Zhang Q, Chu X, Chen T, Ge J, Yu R. Graphene oxide-peptide conjugate as an intracellular protease sensor for caspase-3 activation imaging in live cells. Angew Chem Int Ed Engl 2011;50:7065–9.
[48] Liu Z, Fan AC, Rakhra K, Sherlock S, Goodwin A, Chen X, et al. Supramolecular stacking of doxorubicinon carbon nanotubes for *in vivo* cancer therapy. Angew Chem Int Ed Engl 2009;48:7668–72.
[49] Lee YK, Choi J, Wang W, Lee S, Nam TH, Choi WS, et al. Nullifying tumor efflux by prolonged endolysosome vesicles: development of low dose anticancer-carbon nanotube drug. ACS Nano 2013;7:8484–97.
[50] Robinson JT, Tabakman SM, Liang Y, Wang H, Casalongue HS, Vinh D, et al. Utrasmall reduced graphene oxide with high near-infrared absorbance for photothermal therapy. J Am Chem Soc 2011;133:6825–31.
[51] Elbakry A, Zaky A, Liebl R, Rachel R, Goepferich A, Breunig M. Layer-by-layer assembled gold nanoparticles for siRNA delivery. Nano Lett 2009;9:2059–64.
[52] Akinc A, Thomas M, Klibanov AM, Langer R. Exploring polyethylenimine-mediated DNA transfection and the proton sponge hypothesis. J Gene Med 2005;7:657–63.
[53] Li R, Wu R, Zhao L, Hu Z, Guo S, Pan X, et al. Folate and difunctionalized multiwall carbon nanotubes as dual-targeted drug nanocarrier to cancer cells. Carbon 2011;49:1797–805.
[54] Yang X, Zhang X, Liu Z, Ma Y, Huang Y, Chen Y. High-efficiency loading and controlled release of doxorubicin hydrochloride on graphene oxide. J Phys Chem C 2008;112:17554–8.